

**SYNTHESIS, CHARACTERIZATION, DENSITY  
FUNCTIONAL THEORY ANALYSES AND  
NONLINEAR OPTICAL PROPERTIES OF NEW  
CHALCONE DERIVATIVES**

**DIAN ALWANI BINTI ZAINURI**

**UNIVERSITI SAINS MALAYSIA**

**2020**

**SYNTHESIS, CHARACTERIZATION, DENSITY  
FUNCTIONAL THEORY ANALYSES AND  
NONLINEAR OPTICAL PROPERTIES OF NEW  
CHALCONE DERIVATIVES**

by

**DIAN ALWANI BINTI ZAINURI**

**Thesis submitted in fulfilment of the requirements  
for the degree of  
Doctor of Philosophy**

**May 2020**

## ACKNOWLEDGEMENT

I would like to express my gratitude to Allah SWT for giving me the strength especially during all the challenging moments in completing this thesis.

First and foremost, my heartiest gratitude to my supervisor, Prof. Dr. Abdul Razak Ibrahim, for his patience, continuous supervision, guidance, advice, and support in completing this thesis. I express my humble gratitude to my co-supervisor, Dr. Suhana Arshad for her willingness to spare me her time and guide me in completing my study. They are the backbone of this research with their wonderful suggestions and criticism. I would also like to specially thank Dr. Mundzir Abdullah and the team from the Laser Center, Universiti Teknologi Malaysia for providing the facilities to carry out the NLO experiments for this study.

I would like to dedicate this dissertation to my beloved parents, Zainuri Mat Tapsir and Hapipah Ahmad for all the prayers and sacrifices to make me a successful and better person. Ayah Mak, I hope I have made you both proud. I also would like to convey my appreciation to my lovely siblings, Riean Hidayat Zainuri and Ida Nurani Zainuri for their endless love, support and prayers.

I would like to also thank my dear husband Lt. Kdr. Dauod Ahmad Shamsuddin, for supporting and motivating me to complete this thesis. I am so appreciative for his constant love, understanding, encouragement and for taking care of the family during my busiest hours in completing the thesis. As to my lovely sons, my love for both of them are beyond words. Thank you my 'PHD' sons, Dani Ar Rayyan Dauod Ahmad and Danial Arrash Dauod Ahmad for being my stress relieve pills and always give mommy a source of strength.

To all members and staffs, Mr. Muhammad Fikri Zaini, Ms. Ainizatul Husna Anizaim and Ms. Wong Qin Ai, Mr. Noor Aswafi and Mr. Mustaqim Abu Bakar from the X-Ray Crystallography Lab, School of Physics, for their helps to carry out the experiments for this study.

Last but not least, I would like to thank all my friends for showing their true friendship, care and support when I needed them the most. They are more like a family to me apart from being my research buddies.

My gratitude to Mybrain15 scholarship scheme for funding my studies. Finally, a huge thank you to everyone who has been a part of my life directly or indirectly for their support and prayer.

## TABLE OF CONTENT

<b>ACKNOWLEDGEMENT.....</b>	<b>ii</b>
<b>TABLE OF CONTENTS.....</b>	<b>iv</b>
<b>LIST OF TABLES.....</b>	<b>viii</b>
<b>LIST OF FIGURES.....</b>	<b>x</b>
<b>LIST OF PLATES.....</b>	<b>xvi</b>
<b>LIST OF ABBREVIATIONS.....</b>	<b>xvii</b>
<b>ABSTRAK.....</b>	<b>xix</b>
<b>ABSTRACT.....</b>	<b>xx</b>
<b>CHAPTER 1 INTRODUCTION.....</b>	<b>1</b>
1.1 Nonlinear Optic (NLO) Materials.....	1
1.2 $\pi$ -Conjugated Materials of Chalcone and Anthracene.....	3
1.3 Problem Statement.....	5
1.4 Objectives.....	6
<b>CHAPTER 2 LITERATURE REVIEW.....</b>	<b>7</b>
2.1 Synthesis of Chalcone.....	7
2.2 Fourier Transform Infrared (FTIR) Vibrational Studies.....	8
2.3 Nuclear Magnetic Resonance (NMR) Studies.....	14
2.4 UV-Visible Spectroscopic Studies.....	17
2.5 X-ray Diffraction Studies.....	24
2.6 Quantum Chemical Calculation.....	29
2.6.1 Optimization.....	29
2.6.2 Frontier Molecular Orbital.....	30
2.6.3 Molecular Electrostatic Potential.....	34

2.6.4	Mulliken and Ground State Dipole Moment.....	37
2.7	NLO Characteristic of Chalcone Derivatives.....	40
<b>CHAPTER 3 METHODOLOGY.....</b>		<b>46</b>
3.1	Sample preparation of chalcone derivatives.....	46
3.1.1	Preparation of ( <i>E</i> )-1,3-di(anthracen-9-yl)prop-2-en-1-one ( <b>1</b> )... 47	47
3.1.2	Preparation of ( <i>E</i> )-1-(anthracen-9-yl)-3-(naphthalen-2-yl)prop-2-en-1-one ( <b>2</b> ).....	47
3.1.3	Preparation of ( <i>E</i> )-1-(anthracen-9-yl)-3-(pyren-1-yl)prop-2-en-1-one ( <b>3</b> ).....	48
3.1.4	Preparation of ( <i>E</i> )-1-(anthracen-9-yl)-3-(9-ethyl-9H-carbazol-3-yl)prop-2-en-1-one ( <b>4</b> ).....	48
3.1.5	Preparation of ( <i>E</i> )-3-(4-(9H-carbazol-9-yl)phenyl)-1-(anthracen-9-yl)prop-2-en-1-one ( <b>5</b> ).....	49
3.1.6	Preparation of ( <i>E</i> )-1-(anthracen-9-yl)-3-(4-(dimethylamino)naphthalen-1-yl)prop-2-en-1-one ( <b>6</b> ).....	49
3.1.7	Preparation of ( <i>E</i> )-1-(anthracen-9-yl)-3-(3H-indol-2-yl)prop-2-en-1-one ( <b>7</b> ).....	50
3.1.8	Preparation of ( <i>E</i> )-1-(anthracen-9-yl)-3-(4-(piperidin-1-yl)phenyl)prop-2-en-1-one ( <b>8</b> ).....	50
3.1.9	Preparation of ( <i>E</i> )-1-(anthracen-9-yl)-3-(4-(diphenylamino)phenyl)prop-2-en-1-one ( <b>9</b> ).....	51
3.1.10	Preparation of ( <i>E</i> )-1-(anthracen-9-yl)-3-(2-methoxyphenyl)prop-2-en-1-one ( <b>10</b> ).....	51
3.1.11	Preparation of ( <i>E</i> )-1-(anthracen-9-yl)-3-(3-fluoro-4-methoxyphenyl)prop-2-en-1-one ( <b>11</b> ).....	52
3.1.12	Preparation of ( <i>E</i> )-1-(anthracen-9-yl)-3-(2,4-dichlorophenyl)prop-2-en-1-one ( <b>12</b> ).....	52
3.1.13	Preparation of ( <i>E</i> )-1-(anthracen-9-yl)-3-(2,6-dichlorophenyl)prop-2-en-1-one ( <b>13</b> ).....	53
3.1.14	Preparation of ( <i>E</i> )-1-(anthracen-9-yl)-3-(4-nitrophenyl)prop-2-en-1-one ( <b>14</b> ).....	53

3.1.15	Preparation of ( <i>E</i> )-1-(anthracen-9-yl)-3-(4-iodophenyl)prop-2-en-1-one ( <b>15</b> ).....	54
3.2	Single Crystal X-ray Crystallography.....	55
3.2.1	X-Ray Single Crystal Instrumentation.....	55
3.3	Spectroscopy Studies.....	58
3.3.1	Fourier Transform Infrared Spectroscopy (FTIR) Spectroscopic.....	58
3.3.2	Nuclear Magnetic Resonance (NMR) Studies.....	59
3.3.3	Ultraviolet-Visible (UV-Vis) Studies.....	60
3.4	Density Functional Theory (DFT).....	60
3.5	NLO Investigations.....	61
3.5.1	Linear optical measurement.....	61
3.5.2	Nonlinear optical measurement.....	61
<b>CHAPTER 4</b>	<b>RESULTS AND DISCUSSION.....</b>	<b>65</b>
4.1	X-Ray Structural Analysis.....	65
4.1.1	( <i>E</i> )-1,3-di(anthracen-9yl)prop-2-en-1-one ( <b>1</b> ).....	67
4.1.2	( <i>E</i> )-1-(anthracen-9-yl)-3-(naphthalen-2-yl)prop-2-en-1-one ( <b>2</b> )..	70
4.1.3	( <i>E</i> )-1-(anthracen-9-yl)-3-(pyren-1-yl)prop-2-en-1-one ( <b>3</b> ).....	72
4.1.4	( <i>E</i> )-1-(anthracen-9-yl)-3-(9-ethyl-9H-carbazol-3-yl)prop-2-en-1-one ( <b>4</b> ).....	74
4.1.5	( <i>E</i> )-3-(4-(9H-carbazol-9-yl)phenyl)-1-(anthracen-9-yl)prop-2-en-1-one ( <b>5</b> ).....	77
4.1.6	( <i>E</i> )-1-(anthracen-9-yl)-3-(4-(dimethylamino)naphthalen-1-yl)prop-2-en-1-one ( <b>6</b> ).....	80
4.1.7	( <i>E</i> )-1-(anthracen-9-yl)-3-(3H-indol-2-yl)prop-2-en-1-one ( <b>7</b> ).....	82
4.1.8	( <i>E</i> )-1-(anthracen-9-yl)-3-(4-(piperidin-1-yl)phenyl)prop-2-en-1-one ( <b>8</b> ).....	85
4.1.9	( <i>E</i> )-1-(anthracen-9-yl)-3-(4-(diphenylamino)phenyl)prop-2-en-1-one ( <b>9</b> ).....	87

4.1.10	( <i>E</i> )-1-(anthracen-9-yl)-3-(2-methoxyphenyl)prop-2-en-1-one ( <b>10</b> ).....	89
4.1.11	( <i>E</i> )-1-(anthracen-9-yl)-3-(3-fluoro-4-methoxyphenyl)prop-2-en-1-one ( <b>11</b> ).....	91
4.1.12	( <i>E</i> )-1-(anthracen-9-yl)-3-(2,4-dichlorophenyl)prop-2-en-1-one ( <b>12</b> ).....	93
4.1.13	( <i>E</i> )-1-(anthracen-9-yl)-3-(2,6-dichlorophenyl)prop-2-en-1-one ( <b>13</b> ).....	96
4.1.14	( <i>E</i> )-1-(anthracen-9-yl)-3-(4-nitrophenyl)prop-2-en-1-one ( <b>14</b> )...	97
4.1.15	( <i>E</i> )-1-(anthracen-9-yl)-3-(4-iodophenyl)prop-2-en-1-one ( <b>15</b> ).....	100
4.2	Vibrational Spectroscopic Studies.....	102
4.3	Nuclear Magnetic Resonance (NMR) Spectroscopic Analysis.....	106
4.4	UV-Vis and Frontier Molecular Orbital Studies (FMO).....	112
4.5	Molecular Electrostatic Potential.....	119
4.6	Mulliken and Ground state dipole moment.....	125
4.7	Third Order NLO Studies.....	131
4.7.1	Nonlinear Absorbance (NLA) and Nonlinear Refractive (NLR).....	131
<b>CHAPTER 5 CONCLUSION AND FUTURE RECOMMENDATIONS..</b>		<b>143</b>
5.1	Conclusion.....	143
5.2	Recommendation for Further Research.....	146
<b>REFERENCES.....</b>		<b>147</b>
<b>APPENDICES</b>		
<b>LIST OF PUBLICATIONS</b>		

## LIST OF TABLES

	<b>Page</b>
Table 2.1	Assignment of some characteristic vibrational frequencies..... 9
Table 2.2	<sup>1</sup> H and <sup>13</sup> C isotropic chemical shifts (ppm)..... 14
Table 2.3	The $\lambda_{\text{max}}$ (in nm) and molecular orbital energies (in eV) of some reported studies..... 17
Table 2.4	Third-order nonlinear optical parameter of chalcone derivatives reported by literatures..... 41
Table 3.1	Parameters of z-scan setup..... 62
Table 4.1	Hydrogen bond geometry of <b>1</b> ..... 69
Table 4.2	Hydrogen bond geometry of <b>2</b> ..... 72
Table 4.3	Hydrogen bond geometry of <b>3</b> ..... 74
Table 4.4	Hydrogen bond geometry of <b>5</b> ..... 80
Table 4.5	Hydrogen bond geometry of <b>6</b> ..... 82
Table 4.6	Hydrogen bond geometry of <b>7</b> ..... 84
Table 4.7	Hydrogen bond geometry of <b>8</b> ..... 86
Table 4.8	Hydrogen bond geometry of <b>9</b> ..... 89
Table 4.9	Hydrogen bond geometry of <b>11</b> ..... 93
Table 4.10	Hydrogen bond geometry of <b>12</b> ..... 95
Table 4.11	Hydrogen bond geometry of <b>13</b> ..... 97
Table 4.12	Hydrogen bond geometry of <b>14</b> ..... 99
Table 4.13	Hydrogen bond geometry of <b>15</b> ..... 101
Table 4.14	Vibration results for difference functional groups..... 102
Table 4.15	Experimental and theoretical <sup>1</sup> H and <sup>13</sup> C isotropic chemical shifts (ppm)..... 108

Table 4.16	Experimental and calculated substituent effects on the $\lambda_{\max}$ (in nm) and molecular orbital energies (in eV) of anthracenyl chalcones.....	113
Table 4.17	MEP plot of anthracenyl chalcones .....	119
Table 4.18	The calculated dipole moments (Debye) for all compounds at B3LYP/6-311G++(d,p) level of theory.....	125
Table 4.19	Third-order nonlinear optical parameter of chalcone derivatives.....	132

## LIST OF FIGURES

		<b>Page</b>
Figure 1.1	Synthesis of chalcone.....	3
Figure 1.2	The structure of Anthracene.....	4
Figure 2.1	Synthesis scheme of ( <i>E</i> )-1-(4-Bromophenyl)-3-(naphthalen-2-yl)prop-2-en-1-one (Thanigaimani <i>et al.</i> , 2015).....	7
Figure 2.2	Synthesis scheme of chalcone (Elizabeth <i>et al.</i> , 2006).....	8
Figure 2.3	The scheme of chalcone derivatives labeled at C-H, C=O, C=C and C-C bond.....	8
Figure 2.4	Comparison of FTIR spectrum between difference substituent of anthracenyl chalcone (Maidur <i>et al.</i> , 2018).....	10
Figure 2.5	Compounds of anthracenyl chalcone with different substituents (Prabhakar <i>et al.</i> , 2017).....	10
Figure 2.6	Scheme of ( <i>2E</i> )-1-(5-chlorothiophen-2-yl)-3-(2,3,4-trimethoxyphenyl) prop-2-en-1-one (Kumar <i>et al.</i> , 2015).....	11
Figure 2.7	FTIR spectrum of ( <i>1E,4E</i> )-1,5-di-p-tolylpenta-1,4-dien-3-one (Prasad <i>et al.</i> , 2015).....	12
Figure 2.8	FTIR spectrum of reported structure (Ravindra <i>et al.</i> , 2008).....	13
Figure 2.9	FTIR spectrum of 1-(4-Methoxyphenyl)-3-(3, 4- dimethoxyphenyl)-2-propen-1-one (Shettigar <i>et al.</i> , 2006).....	13
Figure 2.10	The spectrum of (a) <sup>1</sup> H NMR and (b) <sup>13</sup> C NMR (Maidur <i>et al.</i> , 2018).....	15
Figure 2.11	<sup>1</sup> H NMR spectrum of reported compound (Kumar <i>et al.</i> , 2011).....	16
Figure 2.12	The scheme of ( <i>E</i> )-3-(4-(methylsulfanyl)phenyl)-1-(4-nitrophenyl) prop-2-en-1-one (Kumar <i>et al.</i> , 2014).....	17
Figure 2.13	Semiconductor band structure (Zende <i>et al.</i> , 2015).....	18
Figure 2.14	Absorption Spectrum of anthracene (Du <i>et al.</i> , 1998).....	18
Figure 2.15	UV light absorption spectra of anthracene (solid line), CNC-Anthracene (dotted line) and CNCs (dashed line) (Filpponen <i>et al.</i> , 2011).....	19

Figure 2.16	Structure scheme of anthracenyl derivatives (a-e).....	20
Figure 2.17	The experimental absorption spectra of (2 <i>E</i> )-1-(anthracen-9-yl)-3-(4-bromophenyl) prop-2-en-1-one (Br-ANC) and (2 <i>E</i> )-1-(anthracen-9-yl)-3-(4-chlorophenyl)prop-2-en-1-one (Cl-ANC) (Maidur <i>et al.</i> , 2018).....	20
Figure 2.18	The experimental absorption spectra of ( <i>E</i> )-1-(4-aminophenyl)-3-(3-chlorophenyl) prop-2-en-1-one (Ekbote <i>et al.</i> , 2016).....	21
Figure 2.19	UV-Vis absorption spectrum of $1 \times 10^{-5}$ mol.dm <sup>-3</sup> of DBPI in MeOH, DMSO and cyclohexane solvent (Daly <i>et al.</i> , 2014).....	22
Figure 2.20	The electronic absorption of (a) 3-(1-Benzyl-1 <i>H</i> -3-indol-3-yl)-1-naphthalen-2-yl-propenone and (b) 3-(1-Benzyl-1 <i>H</i> -3-indol-3-yl)-1-thiophene-3-yl-propenone with different solvents (Pannipara <i>et al.</i> , 2015).....	23
Figure 2.21	Structure scheme of (a) (2 <i>E</i> )-1-(anthracen-9-yl)-3-(4-bromophenyl)prop-2-en-1-one and (b) (2 <i>E</i> )-1-(anthracen-9-yl)-3-(4-chlorophenyl)prop-2-en-1-one showing the <i>s-trans</i> configuration (Maidur <i>et al.</i> , 2018).....	24
Figure 2.22	Structure scheme of ( <i>E</i> )-1-(anthracen-9-yl)-3-(2-chloro-6-fluorophenyl)prop-2-en-1-one (Abdullah <i>et al.</i> 2016).....	25
Figure 2.23	Different type of configurations of parazolyl chalcone (Parshad <i>et al.</i> , 2015).....	25
Figure 2.24	The molecular structure arranged side by side and linked pairs of weak C—H···O interactions (Kwong <i>et al.</i> , 2017).....	26
Figure 2.25	The donor and acceptor are aligned on a head-to-head alignment (Kwong <i>et al.</i> , 2017).....	26
Figure 2.26	The packing diagram viewed down the <i>a</i> axis (Menezes <i>et al.</i> , 2015).....	27
Figure 2.27	The packing of the molecules down the <i>b</i> axis (Kumar <i>et al.</i> , 2011).....	27
Figure 2.28	ORTEP diagram of the reported molecule (Kumar <i>et al.</i> , 2011).....	28
Figure 2.29	The numbering scheme of reported molecular structure (Custodio <i>et al.</i> , 2018).....	28
Figure 2.30	Frontier molecular orbitals (FMOs) of Br-ANC and Cl-ANC molecules (Maidur <i>et al.</i> , 2018).....	31

Figure 2.31	The HOMO-LUMO gap for different polarity of solvent (Baseia <i>et al.</i> , 2017).....	32
Figure 2.32	The electron density plots of the HOMO LUMO of para-monosubstituted chalcones (Xue <i>et al.</i> , 2010).....	32
Figure 2.33	The energy transition of HOMO-LUMO (Patil <i>et al.</i> , 2017).....	33
Figure 2.34	Transition of energy transfer between HOMO and LUMO (Custodio <i>et al.</i> , 2017).....	34
Figure 2.35	Molecular Electrostatic potential (MEP) of (a) ( <i>E</i> )-1-(4-methoxyphenyl)- 3-(3,4,5- trimethoxyphenyl)prop-2-en-1-one and (b) ( <i>E</i> )-3-(4- ethoxyphenyl) -1-4-methoxyphenyl)prop-2-en-1-one ) (Custodia <i>et al.</i> , 2017).....	34
Figure 2.36	Molecular electrostatic potential surface of benzo and anthraquinodimethane derivatives (a-d) (Abbaz <i>et al.</i> , 2018).....	35
Figure 2.37	Molecular Electrostatic potential (MEP) of (1 <i>E</i> , 4 <i>E</i> )-1-(3-nitrophenyl) phenylpenta-1,4-dien-3-one (Benhalima <i>et al.</i> , 2018).....	36
Figure 2.38	Molecular Electrostatic potential (MEP) of chalcone derivative (Kumar <i>et al.</i> , 2017).....	36
Figure 2.39	The representation of electronic dipole moment vector (blue arrow) based on Milliken population analysis with color scheme for partial charges of chalcone derivatives with different substitution and positions (a) <i>o</i> -OCH <sub>3</sub> , (b) <i>m</i> -OCH <sub>3</sub> , (c) <i>p</i> -OCH <sub>3</sub> , and (d) <i>o,m, p</i> -(OCH <sub>3</sub> ) <sub>3</sub> (Muhammad <i>et al.</i> , 2016).....	38
Figure 2.40	The chemical structure of cyano derivatives (Muhammad <i>et al.</i> , 2016).....	38
Figure 2.41	The scheme of 3,5-di-tert-butyl-4-hydroxybenzoic acid (Mathammal <i>et al.</i> , 2016).....	39
Figure 2.42	The schematic diagram of chemical systems with different hybrid bridging cores (Muhammad <i>et al.</i> , 2014).....	40
Figure 2.43	(a) open and (b) closed aperture Z-scan curve (Maidur <i>et al.</i> , 2018).....	43
Figure 2.44	Optical limiting curve (Maidur <i>et al.</i> , 2018).....	43
Figure 2.45	The molecular structure scheme of 1-(5-chlorothiophene-2-yl)-3-(4-methoxyphenyl) prop-2-en-1-one (Naik <i>et al.</i> , 2015).....	44

Figure 2.46	Open aperture Z-scan curves for 1, 4-Diamino-9,10-Anthraquinone with different concentrations (Zafar <i>et al.</i> , 2013).....	44
Figure 2.47	The molecular structure scheme of (a) ( <i>E</i> )-1-(3-bromophenyl)-3-(4-fluorophenyl)prop-2-en-1-one (F3BC) and (b) ( <i>E</i> )-1-(3-nitrophenyl)-3(4-fluorophenyl)prop-2-en-1-one (F3NC) (Ekbote <i>et al.</i> , 2017).....	45
Figure 3.1	Synthesis of Chalcone.....	46
Figure 3.2	A multiple reflection ATR system (Barbes <i>et al.</i> , 2014).....	58
Figure 3.3	Z-scan technique.....	61
Figure 4.1	(a) The molecular structure of the compound; (b) The optimized structure of the compound at DFT/B3LYP 6-311++G(d,p); (c) The twisted structure of the anthracene units (Anth A and Anth B).....	67
Figure 4.2	Weak C-H $\cdots\pi$ interaction of ( <i>E</i> )-1,3-di(anthracen-9yl)prop-2-en-1-one.....	69
Figure 4.3	a) The molecular structure of the structure; (b) The optimized structure of compound <b>2</b> at DFT/B3LYP 6-311++G(d,p).....	70
Figure 4.4	Weak C—H $\cdots$ O and C—H $\cdots\pi$ interactions of the compound <b>2</b> .....	71
Figure 4.5	a) The molecular structure of the compound <b>3</b> ; (b) The optimized structure of compound <b>3</b> at DFT/B3LYP 6-311++G(d,p).....	72
Figure 4.6	The crystal packing shows C—H $\cdots\pi$ interactions of compound <b>3</b> ... ..	74
Figure 4.7	a) The molecular structure of compound <b>4</b> ; (b) The optimized structure of the compound at DFT/B3LYP 6-311++G(d,p).....	75
Figure 4.8	The crystal packing shows weak $\pi\cdots\pi$ interactions of compound <b>4</b> .. ..	76
Figure 4.9	a) The molecular structure and (b) The optimized structure of the compound at DFT/B3LYP 6-311++G(d,p) .....	77
Figure 4.10	The crystal packing shows weak C—H $\cdots$ O and C—H $\cdots\pi$ interactions of compound <b>5</b> .....	79
Figure 4.11	(a) The molecular structure and (b) The optimized structure of the compound at DFT/B3LYP 6-311++G(d,p).....	80
Figure 4.12	The crystal packing shows weak C-H $\cdots$ O and $\pi\cdots\pi$ interactions of compound <b>6</b> .....	82

Figure 4.13	a) The molecular structure; (b) The optimized structure of compound <b>7</b> at DFT/B3LYP 6-311++G(d,p).....	83
Figure 4.14	Packing diagram showing (a) weak N—H···O and C—H··· $\pi$ interactions of compound <b>7</b> .....	84
Figure 4.15	a) The molecular structure of compound <b>8</b> ; (b) The optimized structure of the compound at DFT/B3LYP 6-311++G(d,p).....	85
Figure 4.16	The crystal packing shows weak C—H···O and C—H··· $\pi$ interactions of compound <b>8</b> .....	86
Figure 4.17	a) The molecular structure of the compound; (b) The optimized structure of the title compound at DFT/B3LYP 6-311++G(d,p).....	87
Figure 4.18	The crystal packing shows weak C—H···O and C—H··· $\pi$ interactions of compound <b>9</b> .....	89
Figure 4.19	a) The molecular structure of compound <b>10</b> ; (b) The optimized structure at DFT/B3LYP 6-311++G(d,p).....	90
Figure 4.20	(a) Crystal packing viewed along the a axis showing weak $\pi$ ··· $\pi$ interactions (dashed lines), where Cg1 and Cg2 are the centroids of the C1–C6 and C18–C22 rings, respectively.....	91
Figure 4.21	a) The molecular structure of compound <b>11</b> ; (b) The optimized structure of the compound at DFT/B3LYP 6-311++G(d,p).....	91
Figure 4.22	Weak C—H···O, C—H··· $\pi$ and $\pi$ ··· $\pi$ interactions (dashed lines) for compound <b>11</b> .....	93
Figure 4.23	a) The molecular structure of compound <b>12</b> ; (b) The optimized structure of the compound at DFT/B3LYP 6-311++G(d,p).....	94
Figure 4.24	Weak C—H···O and C—H··· $\pi$ interactions of the compound.....	95
Figure 4.25	(a)The molecular structure of the compound <b>13</b> ; (b) The optimized structure of the compound at DFT/B3LYP 6-311++G(d,p).....	96
Figure 4.26	Weak C—H···O and C—H··· $\pi$ interactions of the compound.....	97
Figure 4.27	a) The molecular structure of the compound; (b) The optimized structure at DFT/B3LYP 6-311++G(d,p).....	97
Figure 4.28	Packing diagram showing weak C—H···O, C—H··· $\pi$ and $\pi$ ··· $\pi$ interactions of compound <b>14</b> .....	99
Figure 4.29	a) The molecular structure of the compound; (b) The optimized structure at DFT/B3LYP 6-311++G(d,p).....	100

Figure 4.30	The crystal packing shows weak C—H···O interaction of compound <b>15</b> .....	101
Figure 4.31	<sup>1</sup> H and <sup>13</sup> C NMR spectra of compound <b>2</b> .....	106
Figure 4.32	Ring <b>A</b> and Ring <b>B</b> of anthracenyl chalcone derivatives.....	112

## LIST OF PLATES

	<b>Page</b>
Plate 3.1      Bruker APEX II duo CCD diffractometer.....	55

## LIST OF ABBREVIATIONS

A	Acceptor
Anth	Anthracene
ATR	Attenuated Total Reflectance
B3LYP	Becke's nonlocal three parameter exchange and the Lee, Young and Parr
CCD	Charge-Coupled Device
CDCl <sub>3</sub>	Deuteriochloroform
CIF	Crystallographic Information File
CNC	Cellulose Nanocrystals
CSD	Cambridge Structural Database
D	Donor
DFT	Density Functional Theory
DMSO	Dimethyl Sulfoxide
DPSS	Doubled Diode Pumped Solid State
FMOs	Frontier Molecular Orbitals
FTIR	Fourier Transform Infrared
GIAO	Gauge-Invariant Atomic Orbital
HOMO	Highest Occupied Molecular Orbital
ICT	Intermolecular Charge Transfer
KDNB	Potassium 3,5-dinitrobenzoate
KDP	Potassium Dihydrogen Phosphate
KTP	Potassium Titanyl Phosphate
LiNbO <sub>3</sub>	Lithium Niobate
LT	Limiting Threshold
LUMO	Lowest Unoccupied Molecular Orbital

MeOH	Methanol
MEP	Molecular Electrostatic potential
NaOH	Sodium Hydroxide
NLA	Nonlinear Absorption
NLO	Nonlinear Optic
NLR	Nonlinear Refraction
NMR	Nuclear Magnetic Resonance
NOR Lab	Nano-Optoelectronics Research & Technology Laboratory
ORTEP	Oak Ridge Thermal Ellipsoid Plot
Ppm	Parts per million
RSA	Reverse Saturation Absorption
SADABS	Siemens Area Detector Absorption Correction
SAINT	SAX Area-detector Integration (SAX-Siemens Analytical X-ray)
SMART	Siemens Molecular Analysis Research Tools
SHG	Second Harmonic Generation
R	Reliability Index
TD-DFT	Time Dependent Density Functional Theory
TMS	Tetramethylsilane
USM	Universiti Sains Malaysia
UV	Ultraviolet
UV-Vis	Ultraviolet Visible
wR	Weighted Reliability Index

# SINTESIS, PENCIRIAN, ANALISIS TEORI FUNGSI KETUMPATAN DAN SIFAT OPTIK TAKLINEAR TERBITAN KALKON BAHARU

## ABSTRAK

Satu siri sebatian kalkon anthracenil baharu telah berjaya disintesis menggunakan kaedah pemewapan Claisen Schmidt. Struktur terbitan kalkon anthracenyl ini telah ditentukan dan diperhalusi menggunakan data pembelauan hablur tunggal sinar-X dan dioptimakan pada keadaan asas menggunakan kaedah teori fungsi ketumpatan (DFT). Sebatian tersebut kemudiannya dicirikan dengan menggunakan kaedah FTIR, NMR dan UV-Vis. Kehadiran kumpulan berfungsi dan bilangan karbon dan proton dalam struktur molekul telah disahkan oleh spektroskopi FTIR dan NMR, setiap satunya. Spektrum UV-Vis menunjukkan semua kalkon mempunyai panjang gelombang maksima (386-422 nm) yang lebih tinggi dan tetingkap ketelusan yang baik untuk aplikasi optik. Data spektroskopi eksperimen dibandingkan dengan spektrum DFT teori, di mana nilai menunjukkan persetujuan yang baik. Kewujudan ikatan hidrogen intermolekul dalam semua sebatian memainkan peranan penting dalam corak padatan dan sifat NLO. Kesemua sebatian menunjukkan nilai jurang tenaga HOMO LUMO yang baik dan berpotensi untuk aplikasi opto elektronik. Potensi elektrostatik molekul (MEP) mengenal pasti kawasan molekul yang berpotensi mempunyai elektrostatik positif, negatif dan neutral. Gantian yang berbeza pada kalkon anthracenil memberi kesan kepada momen dwikutub dan tindak balas NLO sebatian. Pekali penyerapan taklinear ( $\beta$ ) dan indeks serakan taklinear ( $n_2$ ) telah dinilai dari bukaan terbuka dan tertutup Z-scan. Berdasarkan kiraan kerentanan taklinear  $\chi^3$ , semua struktur menunjukkan potensi aplikasi yang baik seperti aplikasi persuisan optik dan penghad optik.

**SYNTHESIS, CHARACTERIZATION, DENSITY FUNCTIONAL THEORY  
ANALYSES AND NONLINEAR OPTICAL PROPERTIES OF NEW  
CHALCONE DERIVATIVES**

**ABSTRACT**

A series of new anthracenyl chalcone compounds were successfully synthesized using Claisen Schmidt condensation method. These anthracenyl chalcone derivatives structures have been determined and refined using X-ray single crystal diffraction data and optimized at the ground state using density functional theory (DFT) method. The compounds were then characterized by using FTIR, NMR and UV-Vis methods. The presence of functional group and the number of carbon and proton in the molecular structure are confirmed by FTIR and NMR spectroscopy, respectively. The UV-Vis spectrum shows all chalcones have higher maximum wavelength (386-422 nm) and good transparency window for optical application. The experimental spectroscopic data were compared with the theoretical DFT spectra, where the values show good agreement. The existences of intermolecular hydrogen bonds in all compounds play important roles in their packing pattern and NLO properties. All the compounds show a good HOMO-LUMO energy gap values which indicate potential for optoelectronic applications. The molecular electrostatic potential (MEP) identifies the positive, negative and neutral electrostatic potential regions of the molecules. The difference substituents to the anthracenyl chalcone affect the dipole moments and NLO response of the compounds. The nonlinear absorption coefficient ( $\beta$ ) and nonlinear refractive index ( $n_2$ ) have been evaluated from the open aperture and closed aperture Z-scan. Based on the measured nonlinear susceptibility  $\chi^3$ , all structures offers great potential in applications such as optical switching and optical limiting applications.

# CHAPTER 1

## INTRODUCTION

### 1.1 Nonlinear Optic (NLO) Materials

Nonlinear Optical (NLO) is a new area of science and technology playing a major role in modern day hi-tech applications. The use of optical materials has been increased due to their wide range of applications in the field of semiconductors, superconductors and photonics. From materials point of view, NLO materials can be classified into three different categories such as organic, inorganic and semi-organic or metal organic materials (Kanchana *et al.*, 2002). Every class has its own intrinsic advantages for their potential use in NLO applications.

In the beginning, studies were concentrated on inorganic materials such as quartz, potassium dihydrogen phosphate (KDP), lithium niobate ( $\text{LiNbO}_3$ ) and its analogues, potassium titanyl phosphate (KTP) and its analogues (Zhang *et al.*, 2001). KDP is used as a base material to compare second harmonic generation and laser damage threshold values for all crystals. The inorganic NLO materials have some advantages like high melting point, high mechanical strength and compatible physical properties (Hussaini *et al.*, 2009).

The extensive investigations are carried out on organic materials due to their high nonlinearity compared to inorganic materials. Most of the organic molecules consist of extended  $\pi$ -conjugated system end-capped with an electron donor (D) and electron acceptor (A) substituents. The presence of  $\pi$ -delocalized intermolecular charge transfer (ICT) configuration system also exhibit large nonlinear response towards organic molecules (Priyadharshini & Kalainathan, 2018). Some of the advantages of organic materials include flexibility in the method of synthesis, scope

for altering the properties by functional substitution and high damage threshold (Moolya & Dharmaprakash, 2007). Moreover, organic molecules show ultrafast response times, lower dielectric constant, better processability characteristics and enhanced NLO response. A large number of organic materials have been investigated for NLO properties such as chalcone and their derivatives (Shetty *et al.*, 2016), fullerenes (Kost *et al.*, 2005) and hydroxyquinolinium derivatives (Zidan *et al.*, 2016). Organic crystals are widely investigated due to their often high NLO coefficients compared to those of inorganic materials (Hemalatha *et al.*, 2006). Many organic materials shown to have a better nonlinear of opto-electrical properties than inorganic substances (Hameed *et al.*, 2000). They also possess unlimited molecular engineering and can be grown from solution close to room temperature (Zaccaro *et al.*, 1999).

To have strong second order NLO properties, the compound must possess a large first order molecular hyperpolarizability, and also must crystallize in a noncentrosymmetric structure to have a nonzero  $\chi^2$ . In centrosymmetric materials, Second Harmonic Generation (SHG) cannot be demonstrated because of inversion symmetries in polarization and electric field. The only odd terms survive, thus the second order harmonies are not present. The present organic material researches in nonlinear optical field concentrate on both second-order nonlinear optics, which require only occur in molecules that lack a centre of symmetry and third order nonlinear optics which require no symmetrical requirement (Nalwa, 1993). Thus, the range of organic materials with third-order NLO properties are huge. The practical applications of second order and third order NLO materials are very well reported such as in optical data processing, optical limiting and optical data storage applications (Alturk *et al.*, 2016; Patil *et al.*, 2018).

## 1.2 $\pi$ -Conjugated Materials of Chalcone and Anthracene

Chalcones form a group of open-chain flavanoids, in which two aromatic rings are linked by a three-carbon  $\alpha,\beta$ -unsaturated carbonyl system. Chalcones can be prepared by a condensation process between benzaldehyde and acetophenone in the presence of sodium hydroxide as a catalyst (Figure 1.1).

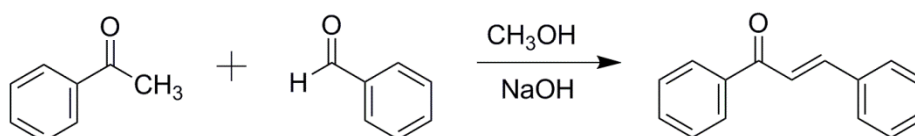


Figure 1.1 Synthesis of chalcone.

Chalcones also have interesting optical properties including high extinction coefficients for absorption in the UV and significant nonlinear response (Zhao *et al.*, 2000). Chalcone compound has a  $\pi$ -conjugated system that provides a large charge transfer axis, which enhances the NLO properties (Ravindra *et al.*, 2007). Chalcones provide suitable configuration for NLO activities with two planar benzene rings connected through a conjugated double bond (Zhao *et al.*, 2000). Chalcones and their derivatives are organic push-pull molecules incorporating polarizable bridge capped by electron donor and acceptor substituent (Janardhana *et al.*, 2013) which are essential for nonlinear activity in organic compound (Kiran *et al.*, 2014).

Anthracene and its derivatives possess interesting photophysical properties and are extremely utilized in the design of luminescent chemosensor and switches (Montalti *et al.*, 2000). Anthracene is a three fused benzene rings sharing common sides (Figure 1.2) polyaromatic hydrocarbons or  $\pi$ -conjugated material with significant conductivity properties that has involved in the progress of organic electronics (Li *et al.*, 2016).

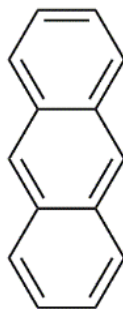


Figure 1.2 The structure of Anthracene.

Anthracenyl-chalcones fulfil the three essential features for high nonlinear activity in an organic compound which are, a strong electron donor, a highly polarizable  $\pi$ -conjugated bridge and a strong electron acceptor (Kiran *et al.*, 2014). Anthracenyl-chalcone with D- $\pi$ -A bridge system is a typical organic NLO material consists of an electron-accepting and electron-donating groups connected by a conjugated bridge allowing good communication between the donor and the acceptor moieties (Minato *et al.*, 2017). The mechanism of  $\pi$ -delocalizing between anthracene and the acceptor via spacer (D- $\pi$ -A) bridge involves long range charge transport phenomenon, including donor-to-ligand and ligand-to-donor transfers. Furthermore, these molecules possess an electron donor group and an electron acceptor contributing to large optical nonlinearity arising from the intramolecular charge transfer (ICT) between the two groups of opposite nature. The design of new systems with high charge transfer is the almost important because intramolecular charge transfer between donor and acceptor will lead to high optical properties (Ekbote *et al.*, 2017). Intramolecular charge-transfer (ICT), such as in D- $\pi$ -A anthracenyl-chalcone molecules can be found in even more distinct optoelectronic properties (Bures, 2014). The electrochemical and spectroscopic properties of these compounds can be modified by adding different substituent to the acceptor group. These types of conjugated material relies on linear electron-rich fragments (Lin *et al.*, 2016).

Significant research in the  $\pi$ -conjugated system has been going on rapidly due to growing number of application in electronic devices such as organic light emitting devices and field effect transistor (Kulkarni *et al.*, 2004; Torrent & Rovira, 2008).

Salsabil *et al.* (2017) studied the effect of substituents on the absorption and fluorescence properties of anthracene. Basically, anthracene derivatives are good candidates for fluorescent probes because they exhibit good emission properties with moderate to high quantum yields (Czamik, 1994; Lakowicz, 2006). In addition, anthracene forms reversible photodimer in response to light and suitable for photochromic applications (Fudickar & Linker, 2010). Due to their suitability for application, anthracene and its derivatives have been studied for their non linear optical properties.

### **1.3 Problem Statement**

In the beginning of NLO studies, many researchers were concentrated on inorganic and other semiconductor materials because they have long been used and are already in the market. Most commercial materials are inorganic especially for high power use. Although inorganic nonlinear optical crystals are easy to grow, but the efficiency of these crystals are lower compared to their organic counterparts. Semiconductors such as gallium arsenide, especially as reduced dimensionality species (quantum wells or quantum wires) possess nonlinear optical effects NLO responses that are among the highest known but the NLO response speed maybe relatively slow (Whittall *et al.*, 1999). Electro-optic devices that use inorganics such as lithium niobate have several drawbacks: high quality single crystals are difficult to grow, are expensive, and not easy to be incorporated into electronic devices (Raposo,

2016). The production of inorganic NLO materials is costly and energy consuming because it requires through purification procedures (Bagher, 2014). Due to the lack of extended  $\pi$ -electron delocalization, purely inorganic materials usually have low NLO responses, difficulty of synthesis, lack of optical quality and slow electro-optic response times (Shi *et al.*, 2017). On the other hand, such materials suffer from disadvantages like modes optical nonlinearity due to the lack of extended  $\pi$ -electron dislocation, absorption in the visible region, poor response time and low laser damage threshold ( $\sim 10 \text{ MWcm}^{-2}$ ) (Zhen *et al.*, 2016).

Therefore, due to many disadvantages of the inorganic materials, there is a prevailing need to investigate the new organic materials and concepts for NLO in order to achieve high NLO efficiency. The synthesis of organic compounds is cheap and gives high yield. Many NLO organic single crystals have been identified as potential candidates in optical and electro-optical devices. The origin of nonlinearity in the NLO material is due to the presence of delocalized  $\pi$ -electron system in organic materials resulting in excellent NLO properties as they can be easily polarized. Chalcone is an organic material having  $\pi$ -conjugated system that can be manipulated as a bridge with a wide range of substitution. The design of new systems with high charge transfer is a key part of this, because intermolecular charge transfer between donor and acceptor will lead to high optical properties (Ekbote *et al.*, 2017).

#### **1.4 Objectives**

1. To synthesize and characterize new chalcone derivatives.
2. To analyze the supramolecular arrangement of the chalcone derivatives.
3. To determine the NLO properties of the chalcone derivatives.
4. To study the structure property relationship of the chalcone derivatives.

## CHAPTER 2

### LITERATURE REVIEW

#### 2.1 Synthesis of Chalcone

Chalcone enables a multiplicity of substitutions on both rings with easy synthesis. There are many types of methods and scheme that are available to synthesis the chalcone. The common types are Claisen Schmidt condensation, Suzuki-Miyaura Coupling reaction, Carbonylative Heck Coupling reaction and Sonogashira Isomerization Coupling. In this research, Claisen Schmidt condensation was used as the synthesis method owing to its simplicity and convenience in this research.

Most of the reported (Kumar *et al.*, 2014; Parlak *et al.*, 2015; Thanigaimani *et al.*, 2015) molecular structures were prepared by the Claisen Schmidt condensation method. The reaction involves cross aldol condensation of benzaldehyde and acetophenone in methanol and the presence of NaOH base as catalyst. The resultant crude products are filtered and crystallized using acetone to get the corresponding chalcone. The synthetic scheme for one of the reported compounds (Thanigaimani *et al.*, 2015) are shown in the Figure 2.1.

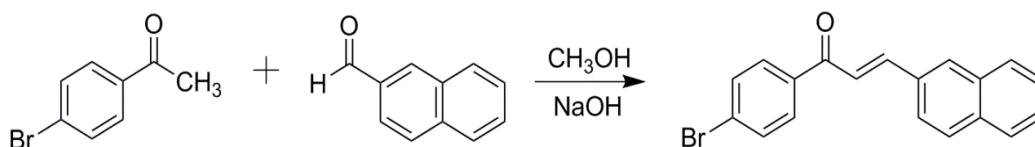


Figure 2.1 Synthesis scheme of (*E*)-1-(4-Bromophenyl)-3-(naphthalen-2-yl)prop-2-en-1-one (Thanigaimani *et al.*, 2015).

Elizabeth *et al.* (2006) synthesized the chalcone (Figure 2.2) using the Claisen Schmidt condensation between acetophenone and benzaldehyde by sonochemical and thermally activated reactions over zeolite as catalyst under solvent free conditions.



Figure 2.2 Synthesis scheme of chalcone (Elizabeth *et al.*, 2006).

Other methods were also reported to have been used successfully to synthesize chalcone derivatives (Selepe *et al.*, 2013; Wu *et al.*, 2010; Braun *et al.*, 2006).

## 2.2 Fourier Transform Infrared (FTIR) Vibrational Studies

The FTIR spectroscopic study is performed to confirm the presence of functional groups in the structural compounds. The spectral range of infrared region covers the frequency range from 400 to 4000  $\text{cm}^{-1}$ . Chalcone derivatives studies are mainly focused on the C-H stretching, C=O stretching, C=C aromatic stretching (Figure 2.3). Reported values of the vibrational frequencies of anthracenyl chalcones from FTIR spectroscopy are tabulated in Table 2.1.

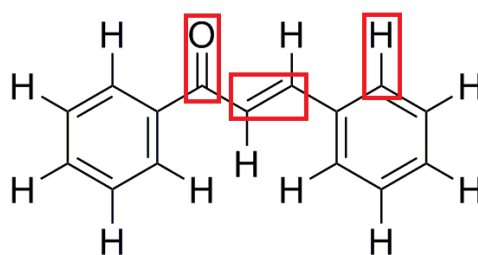


Figure 2.3 The scheme of chalcone derivatives labeled at C-H, C=O, C=C and C-C bond.

Table 2.1 Assignment of some characteristic vibrational frequencies.

Vibrational mode	Experimental (cm <sup>-1</sup> )	Literature
$\nu$ C-H	3023-3263 3120-3131 2992-3132 3068 3000-3125	Maidur <i>et al.</i> (2018) Lavinia <i>et al.</i> (2014) Prabhakar <i>et al.</i> , (2017 ) Prasad <i>et al.</i> (2015) Arunagiri <i>et al.</i> (2015)
<b>In plane C-H</b>	1000-1300	Sri <i>et al.</i> (2012)
<b>Out of plane C-H</b>	749-940	Prasad <i>et al.</i> (2015)
$\nu$ C=O	1640, 1641 1617 1618 1650 1638	Maidur <i>et al.</i> (2018) Lavinia <i>et al.</i> (2014) Prabhakar <i>et al.</i> , (2017 ) Panicker <i>et al.</i> (2015) Kumar <i>et al.</i> 2015
$\nu$ C=C	1200-1670 1520-1598 1576 1608	Maidur <i>et al.</i> (2018) Prabhakar <i>et al.</i> , (2017 ) Kumar <i>et al.</i> 2015 Gallego <i>et al.</i> , 2007
$\nu$ C-C	1460-1642	Lavinia <i>et al.</i> (2014)
<b>Bending C-C</b>	500-1500	Maidur <i>et al.</i> (2018)
$\nu$ C-N	2228	Prabhakar <i>et al.</i> , (2017 )
$\nu$ N-CH	2362	Prabhakar <i>et al.</i> , (2017 )
$\nu$ C-Cl	494,434	Maidur <i>et al.</i> (2018)
<b>Assymmetric <math>\nu</math>CH<sub>3</sub></b>	2919-3016	Siverstain <i>et al.</i> (1981)
<b>Symmetric <math>\nu</math>CH<sub>3</sub></b>	2852	Siverstain <i>et al.</i> (1981)

From the reported studies, most of the C-H stretching vibrations were found to be weak due to the charge transfer from the hydrogen atom to the carbon atom (Prasad *et al.*, 2015; Arunagiri *et al.*, 2015; Maidur *et al.* 2018). The spectrum of anthracenyl chalcones with bromine and chlorine substituents (Maidur *et al.*, 2018) are shown in Figure 2.4. Prabhakar *et al.* (2017) reported 16 compounds of anthracenyl chalcone with different substituents (Figure 2.5). All vibrational mode

values of the 16 compounds were comparable with each other. The region of C-H stretching bands are not affected significantly by nature of the substitutions (Muthu *et al.*, 2015). The CH in-plane bending vibrations usually occur in the region of 1000–1300  $\text{cm}^{-1}$  (Sri *et al.*, 2012) while the CH out-of-plane bending modes generally occur in the region of 749-940  $\text{cm}^{-1}$  (Prasad *et al.*, 2015).

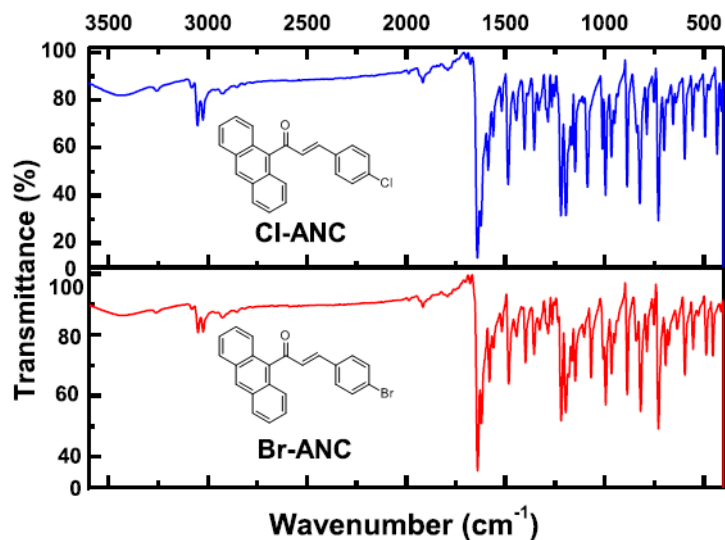


Figure 2.4 Comparison of FTIR spectrum between difference substituent of anthracenyl chalcone (Maidur *et al.*, 2018).

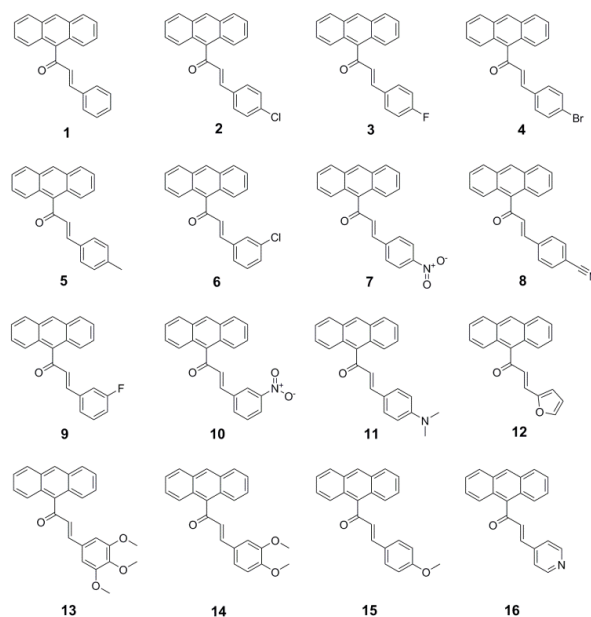


Figure 2.5 Compounds of anthracenyl chalcone with different substituents (Prabhakar *et al.*, 2017).

The wavenumber of the C=O stretch due to carbonyl group mainly depends on the bond strength, which in turn depends upon inductive, conjugative, steric effects and lone pair of electron on oxygen (Panicker *et al.*, 2015). Kumar *et al.* (2015) reported the structure of (2*E*)-1-(5-chlorothiophen-2-yl)-3-(2,3,4-trimethoxyphenyl) prop-2-en-1-one (Figure 2.6) which C=O stretching was observed at 1638 cm<sup>-1</sup> while Prasad *et al.* (2015) reported the value of 1646 cm<sup>-1</sup> (Figure 2.7). The C=O stretching values of 1617-1654 cm<sup>-1</sup> were also reported by other researchers (Maidur *et al.*, 2018; Lavinia *et al.*, 2014; Prabhakar *et al.*, 2017; Panicker *et al.*, 2015). The C=O stretching vibration is also influenced by the intermolecular hydrogen bond between the carbonyl and phenyl groups (Kumar *et al.*, 2014). Additionally, the position of the C=O vibration is very sensitive to various factors like physical state, electronic effects by substituents and ring strains. The formation of conjugated enone of chalcone may shift the wavenumber from the expected ranges (Prasad *et al.*, 2015).

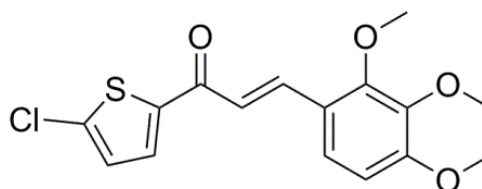


Figure 2.6 The structure of (2*E*)-1-(5-chlorothiophen-2-yl)-3-(2,3,4-trimethoxyphenyl) prop-2-en-1-one (Kumar *et al.*, 2015).

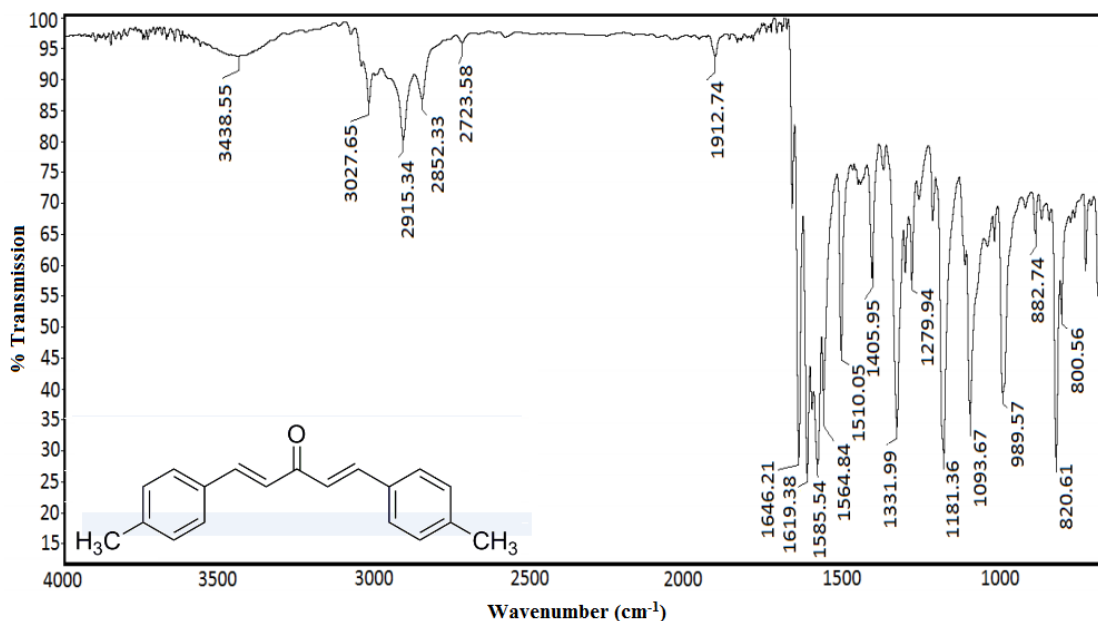


Figure 2.7 FTIR spectrum of (1E,4E)-1,5-di-p-tolylpenta-1,4-dien-3-one (Prasad *et al.*, 2015).

The C=C stretching mode is expected in the region of 1667-1640  $\text{cm}^{-1}$  (Roeges, 1994). According to Socrates (1981), the C=C stretching mode is expected around 1600  $\text{cm}^{-1}$  when conjugated with C=O group. Ravindra *et al.* (2008) concluded that a relatively stronger absorption band at 1597  $\text{cm}^{-1}$  and a weaker absorption band at 1510  $\text{cm}^{-1}$  is due to aromatic ring vibrations and C=C bending modes of  $\alpha$ ,  $\beta$  unsaturated carbons, respectively (Figure 2.8). Shettigar *et al.* (2006) reported the aromatic stretching of C=C assigned at 1588  $\text{cm}^{-1}$  (Figure 2.9). Others studies of anthracenyl chalcone reported the C=C stretching mode in the range of 1200-1670  $\text{cm}^{-1}$  (Maidur *et al.*, 2018; Prabhakar *et al.*, 2017; Kumar *et al.*, 2015; Gallego *et al.*, 2007).

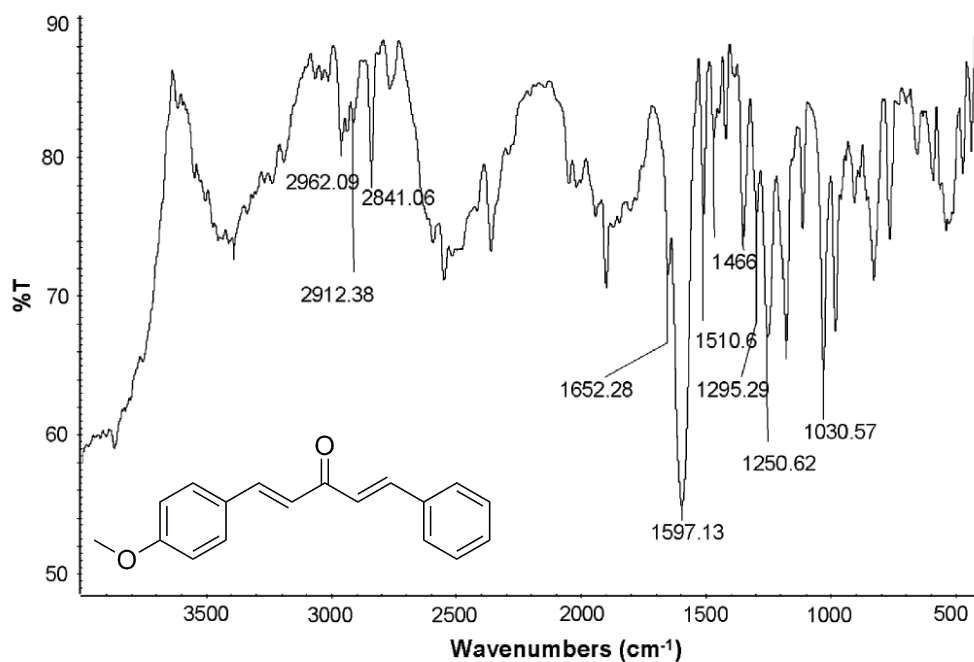


Figure 2.8 FTIR spectrum of reported structure (Ravindra *et al.*, 2008).

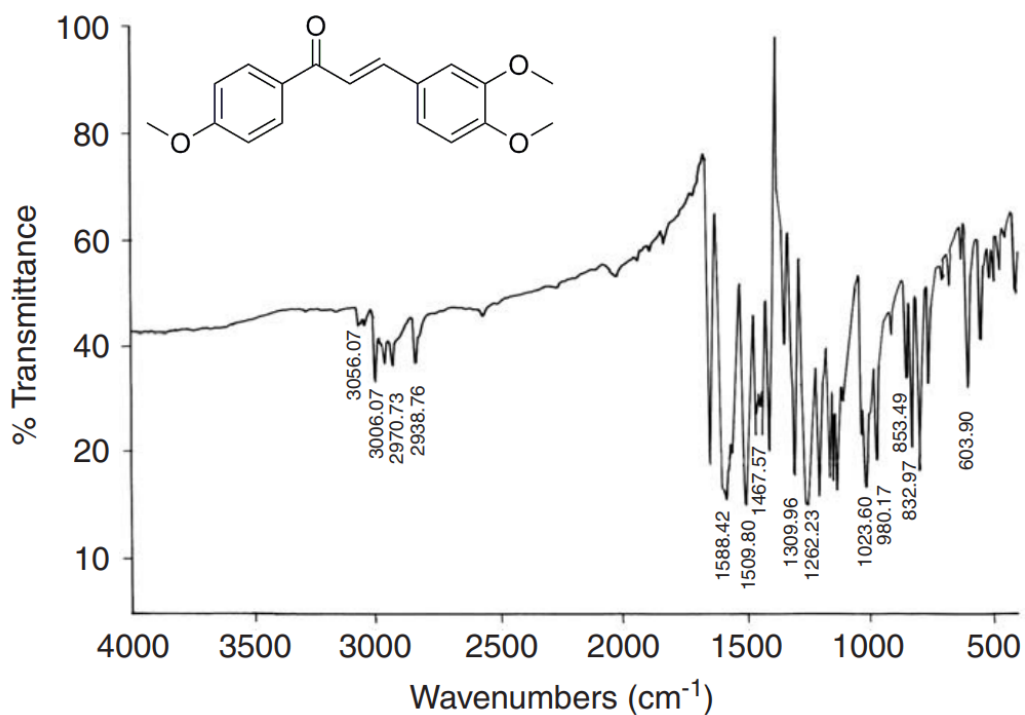
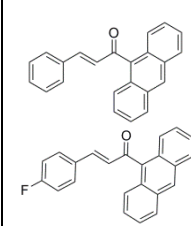
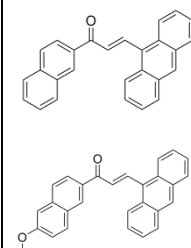
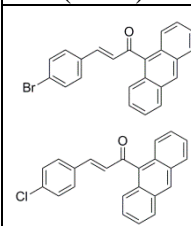


Figure 2.9 FTIR spectrum of 1-(4-methoxyphenyl)-3-(3,4-dimethoxyphenyl)-2-propen-1-one (Shettigar *et al.*, 2006).

### 2.3 Nuclear Magnetic Resonance (NMR) Studies

NMR analyses on similar anthracenyl chalcones have been reported by several studies and tabulated in Table 2.2.

Table 2.2  $^1\text{H}$  and  $^{13}\text{C}$  isotropic chemical shifts (ppm).

Literature	$^1\text{H}$ NMR			$^{13}\text{C}$ NMR	
	$\alpha$	$\beta$	Ar-H	C=O	Ar-H
 Prabhakar <i>et al.</i> (2017)	7.08-7.98	8.04-8.26	7.20-8.55	119.53-200.15	122.43-161.97
 Prakash <i>et al.</i> (2018)	6.80-7.80	7.85-8.45	7.20-8.55	191.55-194.10	111.42-145.32
 Maidur <i>et al.</i> (2018)	7.13-7.18	7.27-7.28	7.22-8.53	199.89	125.17-146.21

The ethylenic double bond hydrogens of the  $\alpha, \beta$  unsaturated system observed as doublet signal in Table 2.2 are due to the  $=\text{CH-CO}$  and  $\text{Ar-CH=C}$  protons of anthracenyl chalcones. The aromatic H for all anthracenyl chalcones show similar range of 7.20-8.55 ppm.

Table 2.2 also shows the C=O which is an electronegative functional group polarizes the electron distribution and shifts to the most deshielded area which is located in the range of 119.53-200.15 ppm. Furthermore, the aromatic carbon signals of all anthracenyl chalcones appeared in the range of 111.42-161.97 ppm.

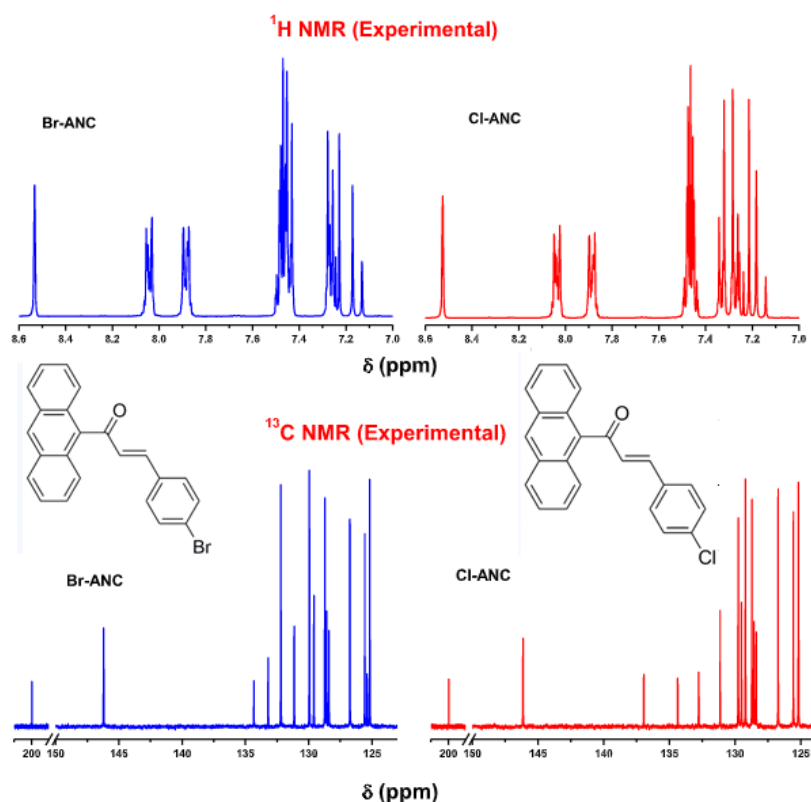


Figure 2.10 The spectrum of (a) <sup>1</sup>H NMR and (b) <sup>13</sup>C NMR (Maidur *et al.*, 2018).

Kumar *et al.* (2011) reported the structure of (*E*)-1-(4-methoxyphenyl)-3-(2,3,5-trichlorophenyl)prop-2-en-1-one (Figure 2.11). The <sup>1</sup>H NMR spectra show the  $\alpha$  (H4) and  $\beta$  (H3) ethylenic bridge protons resonated as two separate doublets centered (Figure 2.11) at 7.45 and 6.87 ppm, respectively. The coupling constant of  $J=9.2$  Hz each confirms the *trans* geometry of the double bond of the reported chalcone. In addition, at the shielded region the protons of methoxy group appeared as a singlet at  $\delta=3.9$  ppm which integrating for three protons.

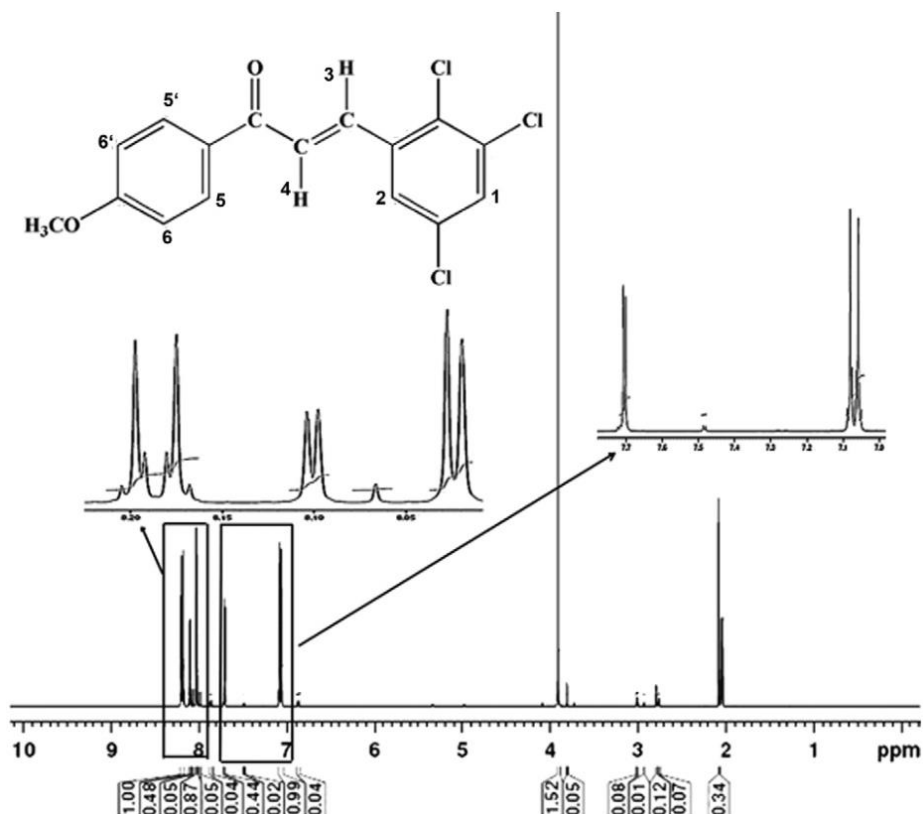


Figure 2.11 <sup>1</sup>H NMR spectrum of reported compound (Kumar *et al.*, 2011).

Kumar *et al.* (2014) reported a chalcone structure having different substituent of electron-withdrawing (Ring 1) and electron-donating (Ring 2) components at the terminal rings (Figure 2.12). The protons of phenyl ring 1 resonated at range 8.25-8.39 ppm, while phenyl ring 2 at 7.69-7.84 ppm. Ring 1 protons appear at a much lower field due to strong electron drawing ability of the nitro group. The hydrogen attached at the electron-withdrawing atom can decrease the shielding and move the resonance of the attached proton towards a higher frequency, whereas the electron-donating increases the shielding and moves the resonance towards a lower frequency (Subramania *et al.*, 2010). For the methoxy substituent, the proton values are  $\leq 3$  ppm due to the shielding effect.

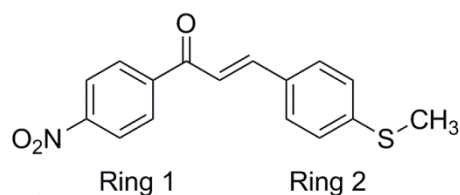


Figure 2.12 The structure of (*E*)-3-(4-(methylsulfanyl)phenyl)-1-(4-nitrophenyl)prop-2-en-1-one (Kumar *et al.*, 2014).

## 2.4 UV-Visible Spectroscopic Studies

Each wavelength of light has a particular energy associated with it. Band gap is the energy difference between the top of the valence and conduction band (Figure 2.13). In order for an electron to jump from a valence band to a conduction band, it requires a specific minimum amount of energy for the transition. Table 2.3 shows the maximum absorbance peak and energy gap of some reported studies of some anthracenyl chalcones.

Table 2.3 The  $\lambda_{\max}$  (in nm) a molecular orbital energies (in eV) of some reported studies.

Literature	Absorption maximum (nm)	Energy gap (eV)
Zende <i>et al.</i> (2015)	360-400	2.95
Maidur <i>et al.</i> (2018)	366, 370	2.75, 2.81
Ekbote <i>et al.</i> (2017)	366	2.96
Kumar <i>et al.</i> (2017)	364	3.02

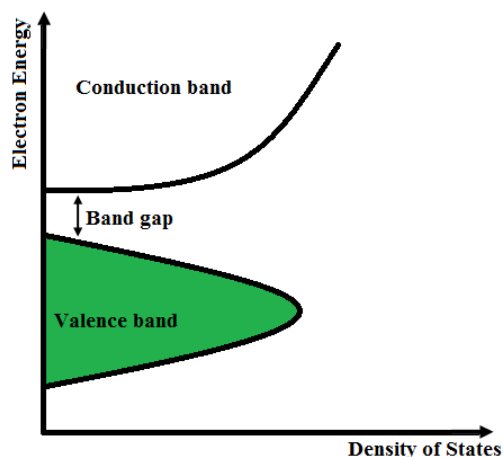


Figure 2.13 Semiconductor band structure (Zende *et al.*, 2015).

The conjugated system such as anthracene derivatives has a large influence on peak wavelengths and absorption. With the larger conjugated system, the absorption peak wavelengths tend to shift towards the long wavelength region and the absorption peaks tend to be larger (Masayoshi, 2002). Figure 2.14, shows the absorption spectrum pattern of anthracene in cyclohexane as reported by Du *et al.* (1998).

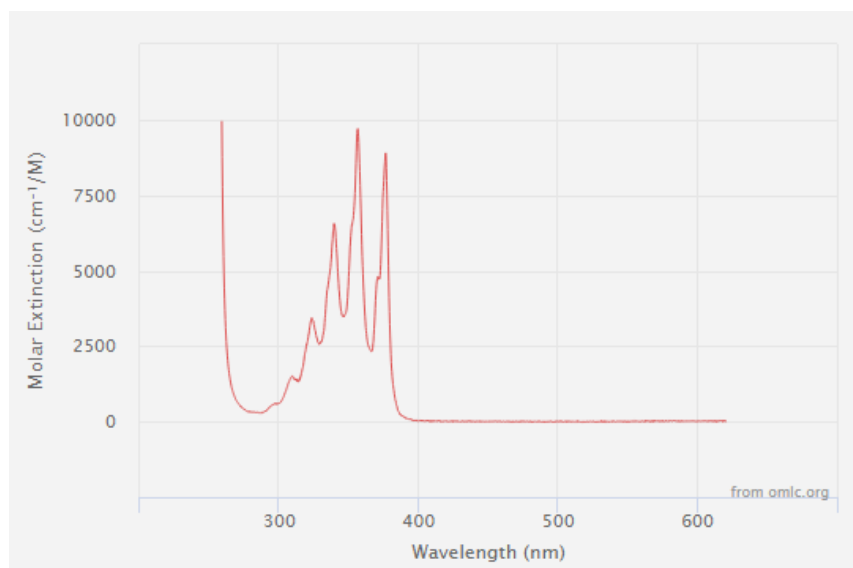


Figure 2.14 Absorption Spectrum of anthracene (Du *et al.*, 1998).

Filpponen *et al.* (2011) reported UV light absorption spectra of cellulose nanocrystals (CNC), anthracene and cellulose nanocrystal anthracene (CNC-Anthracene) (Figure 2.15). Anthracene has a typical UV light absorption bands at 392 nm, 372 nm, 355 nm and 338 nm. From the spectrum, it reveals that anthracene with the substituent of CNC have similar pattern of absorption bands with the anthracene, while the unmodified CNC have no UV absorption observed. It also shows that the effect of substituents plays an important role in the UV spectrum. Furthermore, the peaks in the anthracene spectrum are due to vibrational transitions of conjugated system in addition to the electronic transition forming the excited state.

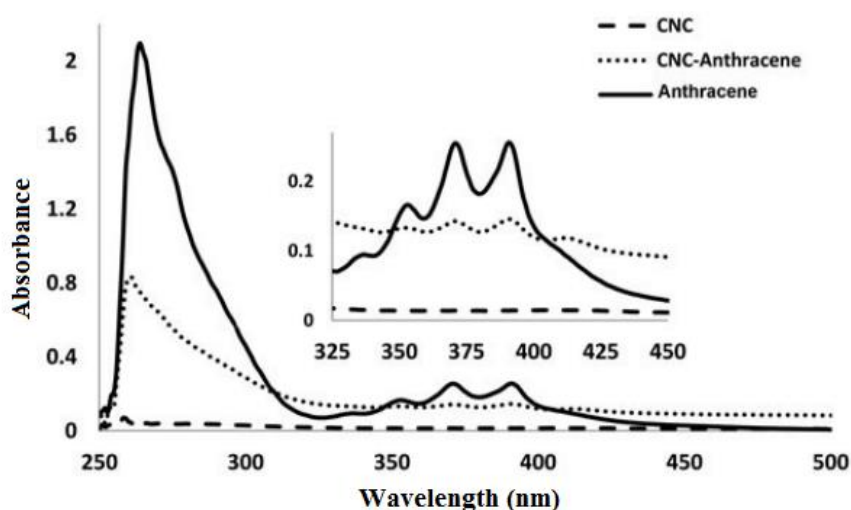


Figure 2.15 UV light absorption spectra of anthracene (solid line), CNC-Anthracene (dotted line) and CNCs (dashed line) (Filpponen *et al.*, 2011).

Zende *et al.* (2015) also reported the structure of large conjugated system, anthracene derivatives (Figure 2.16) which showed absorbance values in the range of 360-400 nm with the molecular energies of around 2.95 eV. Maidur *et al.* (2018) described two new structures of anthracenyl chalcones which spectrum (Figure 2.17) consisting of higher maximum absorbance at 366 and 370 nm. The absorbance

maxima is assigned to the  $\pi$ - $\pi^*$  transitions. The optical energy gaps were estimated by extrapolation linear line and gave the values of 2.75, 2.81 eV. The semi-organic single crystal of potassium 3,5-dinitrobenzoate (KDNB) reported by Karuppasamy *et al.* (2016) shows the energy band gap of 3.20 eV and is considered to possess good optical behavior for practical applications.

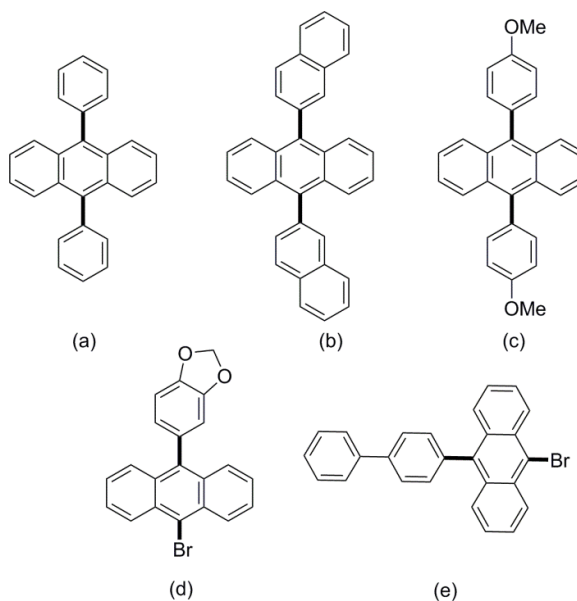


Figure 2.16 Structure of anthracenyl derivatives (a-e) (Zende *et al.*, 2015).

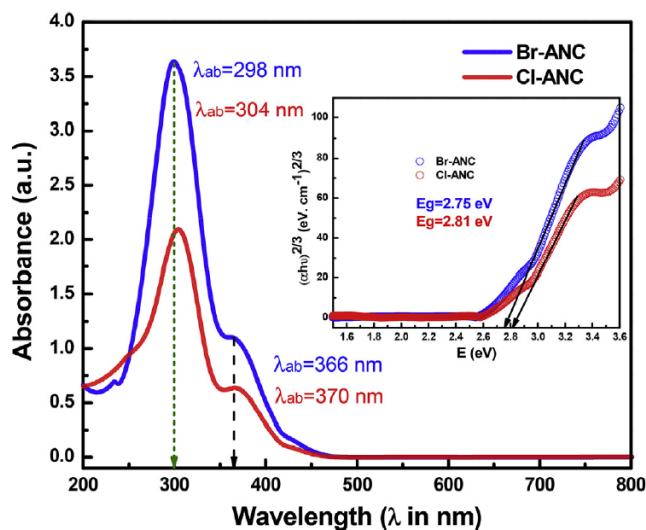


Figure 2.17 The experimental absorption spectra of (2*E*)-1-(anthracen-9-yl)-3-(4-bromophenyl)prop-2-en-1-one (**Br-ANC**) and (2*E*)-1-(anthracen-9-yl)-3-(4-chlorophenyl)prop-2-en-1-one (**Cl-ANC**) (Maidur *et al.*, 2018).

Ekbote *et al.* (2017) reported a halogenated chalcone with chlorine substituent showing maximum peak of 366 nm (Figure 2.18) and energy gap of 2.96 eV. The corresponding values involving bromine substituent are 364 nm and 3.01 eV, respectively (Kumar *et al.*, 2017). The bathochromic shift depends on the electronegativity of the halogen substituents (Berens & Shugar, 1963). The halogen substituents also affects the optical absorption bands of a compound (Lohmann, 1974; Zaini *et al.*, 2019).

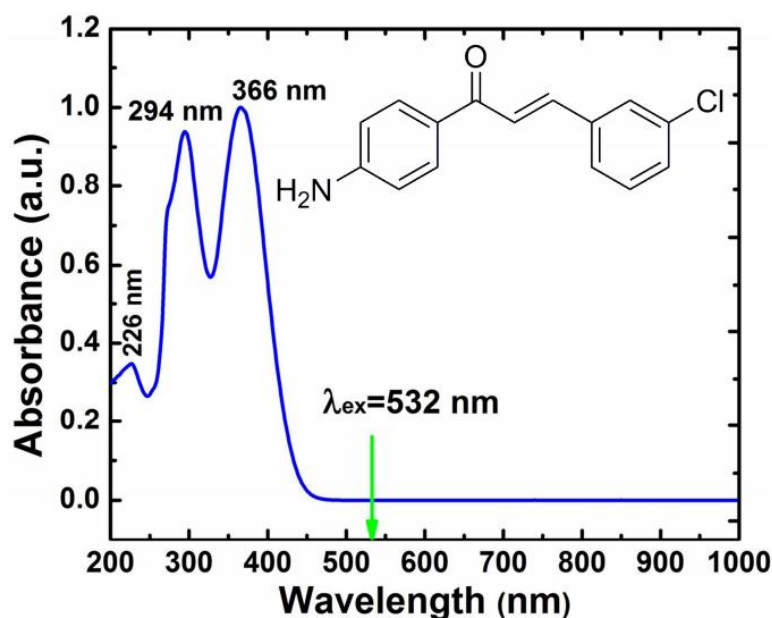


Figure 2.18 The experimental absorption spectra of (*E*)-1-(4-aminophenyl)-3-(3-chlorophenyl) prop-2-en-1-one (Ekbote *et al.*, 2016).

Daly *et al.* (2014) studied the effect of three solvents which are methanol (MeOH), dimethyl sulfoxide (DMSO) and cyclohexane on the UV Vis absorption (Figure 2.19). The absorption spectra shift to the higher maximum wavelength with increasing solvent polarity. This is due to the attractive polarization forces between the solvent and absorber, which determine the decrease of ground and excited states energy.

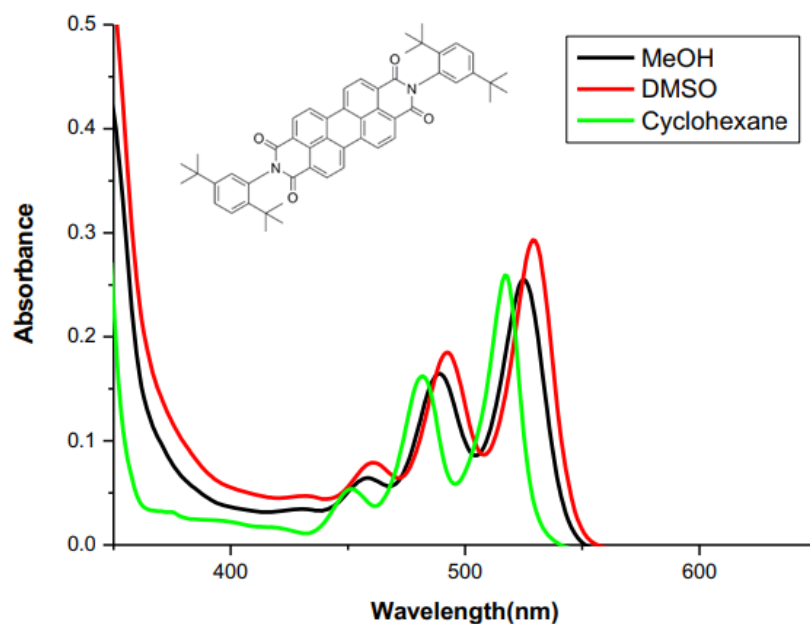


Figure 2.19 UV-Vis absorption spectrum of  $1 \times 10^{-5} \text{ mol.dm}^{-3}$  of N, N-Bis (2, 5-di-tert-butylphenyl)-3, 4:9,10-perylenebis (dicarboximide) in MeOH, DMSO and cyclohexane solvent (Daly *et al.*, 2014).

Pannipara *et al.* (2015) reported two chalcones, 3-(1-Benzyl-1H-3-indol-3-yl)-1-naphthalen-2-yl-propenone and 3-(1-Benzyl-1H-3-indol-3-yl)-1-thiophene-3-yl-propenone with electron donating and accepting groups attached. Figure 2.20 shows the red shift is observed in the absorption maxima from heptanes to methanol which is increasing from non polar to polar solvent. Both compounds show very strong solvent polarity dependent changes where the red shift in absorption spectra occurs with the increasing solvent polarity.

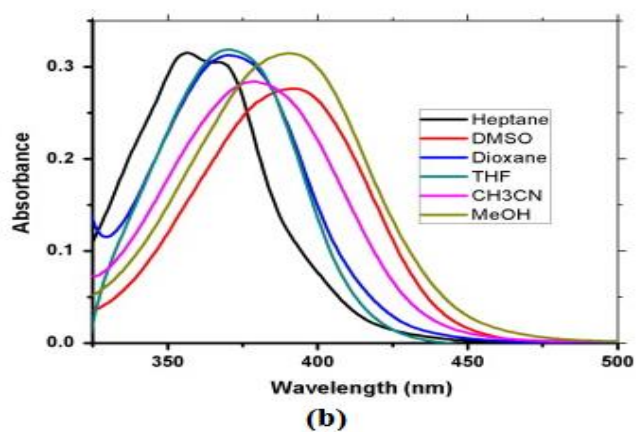
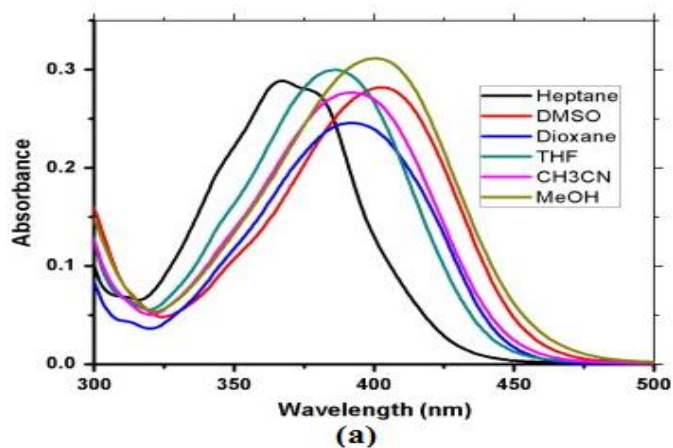


Figure 2.20 The electronic absorption of (a) 3-(1-Benzyl-1H-3-indol-3-yl)-1-naphthalen-2-yl-propenone and (b) 3-(1-Benzyl-1H-3-indol-3-yl)-1-thiophene-3-yl-propenone with different solvents (Pannipara *et al.*,2015).

## 2.5 X-ray Diffraction Studies

Each molecular structure usually has different character and properties designated as *cis*, *trans*, *s-trans* and *s-cis* configurations. Usually, the molecular structure of chalcones are *trans* configured. Maidur *et al.* (2018) reported the *trans* configuration of (2*E*)-1-(anthracen-9-yl)-3-(4-bromophenyl)prop-2-en-1-one and (2*E*)-1-(anthracen-9-yl)-3-(4-chlorophenyl)prop-2-en-1-one (Figure 2.21). The bulkiness of the anthracene ring gives rise to a highly twisted structure at the terminal ring. Meanwhile, the molecular structure of (*E*)-1-(anthracen-9-yl)-3-(2-chloro-6-fluorophenyl)prop-2-en-1-one (Abdullah *et al.*, 2016) shows the enone moiety locked in a *trans* configuration (Figure 2.22) originated from an intramolecular hydrogen bond which generates an *S*(6) ring motif (Figure 2.22). Other types of configurations such as *s-cis* (*E*), *s-trans* (*E*), *s-cis* (*Z*) and *s-trans* (*Z*) (Figure 2.23) are also reported.

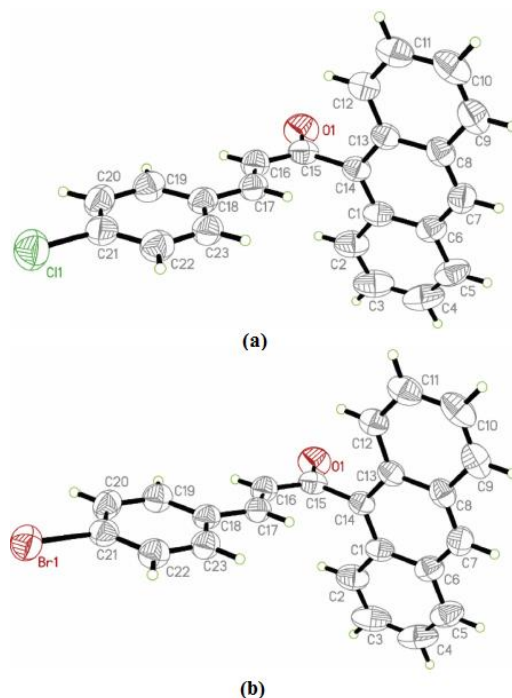


Figure 2.21 Structure (a) (2*E*)-1-(anthracen-9-yl)-3-(4-bromophenyl)prop-2-en-1-one and (b) (2*E*)-1-(anthracen-9-yl)-3-(4-chlorophenyl)prop-2-en-1-one showing the *s-trans* configuration (Maidur *et al.*, 2018).